Nanoscale

ROYAL SOCIETY OF CHEMISTRY

PAPER

View Article Online
View Journal | View Issue

Check for updates

Cite this: *Nanoscale*, 2023, **15**, 5414

Graphene nanoplatelets and other 2D-materials as protective means against the fading of coloured inks, dyes and paints†

M. Kotsidi,[a,b] G. Gorgolis, [a,b] M. G. Pastore Carbone, [a] G. Paterakis, [a] G. Anagnostopoulos, [a] G. Trakakis, [a] A. C. Manikas, [b] C. Pavlou,[a] N. Koutroumanis[a] and C. Galiotis [*a,b]

The present work demonstrates the ability of graphene nanoplatelets (GNPs) and other two-dimensional materials (2DMs) like tungsten disulfide (WS_2), molybdenum disulfide (MoS_2) and hexagonal boron nitride (hBN) to act as protective barriers against the fading of architectural paints and also inks/paints used in art. The results present a new approach for improving the lightfastness of colours of artworks and painted indoor/outdoor wall surfaces taking advantage of the remarkable properties of 2DMs. As shown herein, commercial inks and architectural paints of different colours doped with graphene nanoplatelets (GNPs), graphene oxide (GO), reduced graphene oxide (rGO) and other 2DMs, exhibit a superior resistance to fading under ultraviolet radiation or even under exposure to visible light. A spectroscopic study on these inks and dyes reveals that the peaks which are characteristic of the colour pigments are less affected from aging/fading when the GNPs and the other 2DMs are present. The protection mechanism for the GNPs and the other 2DMs differs. For GNPs, mainly their high surface area which leads to free radicals scavenging (especially hydroxyl radicals), and secondarily their UV absorption, are responsible for their protection effects, while for GO, a transition to rGO structures and consequently to '*smart*' paints can be observed after the performed aging routes. In this way, the paint gets improved by time preventing or slowing its own fading and decolorization. For the other 2DMs, the transition-metal dichalcogenides performed better than hBN, even though they all absorb in the UV region. This can be ascribed to the facts that the formers also absorb in the visible, while hBN does not, while most importantly, they can trap reactive oxygen species (ROS) and corrosive gases in their structure as opposed to hBN. By conducting colorimetric measurements, we have discovered that the lifetime of the as-developed 2DM-doped inks and paints can be extended by up to ~40%.

Received 18th October 2022,
Accepted 17th February 2023

DOI: 10.1039/d2nr05795f

rsc.li/nanoscale

Open Access Article. Published on 23 February 2023. Downloaded on 8/16/2024 2:06:04 PM.
This article is licensed under a Creative Commons Attribution-NonCommercial 3.0 Unported Licence.

Introduction

The selective reflection of visible light by dyes results in their corresponding colours. But, at the same time, absorbed photons from a dye, especially those having higher energy, can excite molecules from the ground state, triggering a series of chemical reactions resulting in colour degradation or fading. In light of that, the exposure of colours used in artworks to ultraviolet (UV) and visible light in the presence of oxidizing agents, initiates colour changes, fading and yellowing.[1] Unfortunately, this degradation consequently results in the irreversible alteration of artworks which are precious crafts that must also pass on to future generations. A notable example that has been recently reported[2] is the colour change of Van Gogh's 'Sunflowers', in which lead crystals of red colour have turned into white plumbonacrite due to the reaction of paint impurities with light and CO_2. Also, it was found that a certain pigment – *i.e.* cadmium yellow – was reacting with sunlight and degrading to another beige compound.[3] Another painting by van Gogh, 'Flowers in a Blue Vase', has also been badly affected.[3] Many artistic paintings are at risk due to this process. Similarly, architectural paints and coatings are known to be degraded mainly due to photo-corrosion and photo-oxidation.[4,5] Photodegradation processes induce irreversible colour alterations that cannot be easily predicted or prevented. An ideal architectural paint or coating should demonstrate high resistance to UV radiation, good adhesion and durability, high resistance to moisture, low tendency for soiling, low permeability to gaseous pollutants *e.g.*, CO_2 (anti-

[a]*Institute of Chemical Engineering Sciences, Foundation for Research and Technology – Hellas (FORTH/ICE-HT), Patras 265 04, Greece.*
E-mail: c.galiotis@iceht.forth.gr
[b]*Department of Chemical Engineering, University of Patras, Patras 26504, Greece*
† Electronic supplementary information (ESI) available. See DOI: https://doi.org/10.1039/d2nr05795f

This journal is © The Royal Society of Chemistry 2023

Open Access Article. Published on 23 February 2023. Downloaded on 8/16/2024 2:06:04 PM.
This article is licensed under a Creative Commons Attribution-NonCommercial 3.0 Unported Licence.

carbonation properties) and anti-fungal properties without or with reduced use of biocides, thus protecting the aquatic horizon from biocides that have been swept away by rainwater from the painted surface (leaching).[6] All these features, in tandem with water-based formulations, are expected to foster sustainable paints with higher protection and durability, lower maintenance costs for the surfaces to be applied from these products and at the same time they will possess a reduced environmental footprint as they will prevent wasteful and inefficient use of energy and material resources from start to finish.

Since its isolation in 2004,[7] graphene has been termed as the "wonder material" due to its outstanding chemical resistance,[8] ability to conduct heat and electricity[9,10] and excellent physical/mechanical properties.[11,12] In addition, the fact that graphene and its related materials (GRMs) appear as non-toxic is also an important finding.[13] In the absorption spectrum, monolayer graphene exhibits an asymmetric broad peak at 270 nm, and considering that the reflectance is negligible, its UV absorbance can reach ~8%. In the visible part of the spectrum, a single layer graphene can absorb ~2.3% of incident light, transmitting the remaining ~98%.[14,15] In the UV range, where optical transitions of these π-bands approach the so-called "saddle" point singularity of the Brillouin zone,[16] the inter-band optical absorbance increases far beyond a standard value[15] and exhibits excitonic effects. In that spectral segment, the optical conductivity shows a single broad peak at photon energy equal to 4.62 eV which correspond to a wavelength equal to 268 nm. This feature makes GRMs promising candidates for UV protection, as they can cover a much broader absorbance region than just a sharp peak, providing thus a remarkable protection for both UVC (100–280 nm) and UVB (280–315 nm).[17,18] In particular, graphene nanoplatelets (GNPs), which are nanoparticles comprised of short stacks of platelet-shape graphene sheets, with low thickness and an average lateral size of up to 50 microns, have been employed as UV absorbers or UV blockers in several applications.[19,20]

Graphene oxide (GO), another graphene derivative, is an abundantly available and low-cost carbon compound that contains a cluster of reactive oxygen functional groups.[21] It can be synthesized from graphite or graphite oxide[22] by employing the Brodie, Staudenmaier, Hummers' method or its modification.[23] GO can interact with a broad range of organic and inorganic materials,[24] is highly hydrophilic, and can form stable aqueous colloids to facilitate the assembly of macroscopic structures by simple and cheap solution processes. GO has been also exploited in improving the protection from UV radiation in composites. Tang *et al.*[19] synthesized a multifunctional cotton fabric with high electrical conductivity and strong UV radiation protection by using GO dispersion onto the fabric *via* vacuum filtration deposition and afterwards treating with polyaniline. Also, Hu *et al.*[25] incorporated GO as functional nanofiller into sodium alginate *via* solvent-casting and achieved high UV shielding and mechanical performance simultaneously. GO can also be reduced chemically or thermally in order to achieve graphene like properties.[26] In addition to above synthetic routes, it has been reported[27,28] that the reduction of GO in water could be also implemented by UV light. In fact, after UV irradiation, a decrease of oxygen bonded to carbon and a restoration of the extended conjugated sp^2 structure[28] are observed. Thus, the reduction of aqueous GO dispersions at ambient conditions with intense UV light could be an alternative to reduction induced by chemical reactants, high temperature and/or catalysts.

The exploitation of graphene and its related materials for the protection against fading or bleaching of colours and photographs is a newly emerging field. Recently, our group[29] has shown that a single-layer or multilayer graphene veil, produced by chemical vapour deposition, can be deposited over artworks to protect them efficiently against colour fading, with a protection factor of up to 70%. Another example is the use of graphene-enhanced coatings for colour protection of wall painting, which has been proposed by Zhu *et al.* and is based on the exploitation of $Ca(OH)_2$/graphene quantum dot nanohybrids.[30] Other 2-dimensional materials (2DMs) like tungsten disulfide (WS_2), molybdenum disulfide (MoS_2) and hexagonal boron nitride (hBN) are known to absorb in the UV part of the electromagnetic spectrum[31–33] and therefore are promising candidates against the fading of inks and dyes. Still, it is important to note here that one critical issue for the exploitation of graphene and other 2DMs is to obtain a successful liquid phase exfoliation by using as less harmful and toxic solvent as possible.[34,35]

Herein we demonstrate that GNPs, GO and other 2DMs can be successfully exploited to endow paints used both in art and architecture/buildings with intrinsic anti-fading properties and even other multifunctionalities. With an eye on sustainability, we formulated eco-friendly, water-based dispersions of well-exfoliated GRMs and 2DMs that, dispersed to inks and paints, prevent colour degradation thus enhancing the lightfastness and the durability. In this regard, graphene flakes dispersed to colour paints bestow enhanced UV, oxidation and humidity resistance, while the other examined 2DMs seem to offer protection against UV and visible light as well. Eventually, we demonstrate that we can take advantage from the 'green' reduction of GO through irradiation-assisted approach to avoid decolourization of the paints. Actually, without using extra chemicals or elevated temperatures, which are the standard methods for GO reduction to produce reduced GO (r-GO), the UV/visible irradiation of a GO target in water is found here to be an alternative route for triggering the chemical reduction. The *in situ* reduction of GO at the surface or near-surface of the paint during its exposure to radiation, is thus demonstrated to increase the protection ability of the material against fading and decolourization.

Experimental

Materials

Dispersions of GNPs and other 2DMs. Graphene nanopowder (Elicarb Electrical grade, gently supplied by Thomas

Open Access Article. Published on 23 February 2023. Downloaded on 8/16/2024 2:06:04 PM.
This article is licensed under a Creative Commons Attribution-NonCommercial 3.0 Unported Licence.

Swan & Co. Ltd) was adopted in this study. Graphene oxide was synthesized from natural graphite flakes (NGS Naturgraphit GmbH, Germany) by a two-step oxidation process[36] where single and few layers of GO were collected by a combination of ultra-sonication and centrifugation steps (see ESI† for more). Commercial hBN ('Thomas Swan', 20 g), WS_2 ('Sigma Aldrich', 50 g, 2 μm, 99%) and MoS_2 ('Sigma Aldrich', 100 g) powders were also used for the needs of this study.

Commercial powders of GNPs and other 2D materials were exfoliated in a binary mixture of water–ethanol. Initially, mechanical exfoliation with mortar and pastel was applied to the bulk powder with suitable solvent to break down and exfoliate the thickest flakes. Then, a solution of 1 mg ml^{-1} of GNPs in water/ethanol with ethanol molar fraction equal to 0.06 was exfoliated through bath sonication (ElmaS30 Elmasonic) for 3 hours or shear mixing (Silverson L5M) at 5000 rpm for 20 min. In both cases, the resultant dispersion was then centrifuged, using a Hettich Mikro 22R centrifuge for 10 minutes at 1000 rpm, to separate the bulk flakes from the exfoliated ones (supernatant) by decantation with a pipette, and then the collected supernatant solution was centrifuged again for 5 minutes at 6000 rpm to collect the exfoliated graphene flakes from the bottom of the falcon in the form of dense, paste-like, solution. For the cases of WS_2, MoS_2 and hBN, the mole fraction of ethanol-in-water solution employed for the exfoliation was equal to 0.06, 0.04 and 0.04, correspondingly. From the first attempt of exfoliating these materials with shear mixing, only breaking of the flakes was observed without a significant decrease of the number of their layers. Consequently, the next round of exfoliation of the prepared solutions was performed with the aim of a bath sonicator for 3 hours.

Preparation of inks and paints doped with GNPs and other 2DMs. Commercial blue, pink and green drawing inks (ultramarine, carmine and deep green, Pelikan), yellow acrylic paint (Royal Talens acrylic), red and yellow architectural paints (Kraft PAINTS, Master™ Basics, Red/Yellow 180 ml) were used in this work. Tartrazine (Sigma-Aldrich, product number: T0388) in a 2.5% (w/w) aqueous solution and methylene blue (Sigma-Aldrich, product number: M9140) in a 0.001 mg ml^{-1} aqueous solution were also used in this study. Dispersions of GNPs and of the other 2DMs produced *via* liquid phase exfoliation were added to commercial inks, dyes and other paints through mixing with mortar and pestle for 3 minutes *ca.* Similarly, for the production of GO-based inks, the graphene oxide solution with a known concentration (3.2 mg ml^{-1}) in water was weighed, and then incorporated *via* mortar and pestle. Tartrazine solution and the inks were then applied on the Bristol type cardboard substrates using the doctor blade technique. Samples were left to dry under the hood for 24 hours. Architectural paints were deposited on plasters by drop-castings. Control samples were also produced by painting the substrates (either cardboard or plasters) with bare dyes and paints.

Characterization methods

In order to examine the structural characteristics of the powders and their graphitic nature, scanning electron microscopy (SEM) and Raman spectroscopy were employed. SEM photos were taken by a LEO SUPRA 35 VP, while Raman spectra of the powders were recorded by an InVia Reflex (Renishaw, UK) MicroRaman equipment using a 514 nm laser excitation. Raman spectroscopy was adopted for spectroscopic characterization of the materials at different stages of this study, namely the material preparation, the investigation of the degradation mechanism and the durability of graphene upon exposure to UV light. In all experiments, spectra were recorded at several points on each specimen using a Renishaw InVia Raman Spectrometer with a 1200 grooves per mm grating and a ×100 lens. The power of the laser beam was kept below 1 mW to avoid heating of the specimen. Raman spectra were baseline corrected and graphene peaks were fitted to Lorentzian functions. When graphene peaks were superimposed onto the peaks of the substrates, the necessary deconvolution process was applied. In this analysis, the Lorentzian components assigned to the substrates were held fixed, having had their parameters (position, full-width at half-maximum) evaluated from the spectra of the bare substrates.

A HP 8452A Diode Array spectrophotometer was used for obtaining the relevant spectra of samples with and without graphene. A light ray of wavelength from 200 to 800 nm was used as a source. The standard quartz cuvette with dimension of 10 mm × 10 mm × 45 mm and thickness of about 1.2 mm of was used as liquid container for this measurement.

Colorimetric coordinates are extracted from reflectance spectra using standard illuminant D65 and a standard observer at 10° (CIE 1964). The colour difference for each specimen can be expressed in terms of the ΔE^* parameter, calculated from the colorimetric coordinates and L^*, a^*, and b^* as follows:[37]

$$\Delta E = \sqrt{(L_2^* - L_1^*)^2 + (a_2^* - a_1^*)^2 + (b_2^* - b_1^*)^2} \quad (1)$$

ΔL, Δa and Δb represent the luminosity change, red-green and the blue-yellow parameter respectively. It is worth noting that a ΔE^* around than 2.3 units makes the colour difference just perceivable by the naked eye.[37] In our experiments, reflectance spectra were acquired using an FRU WR-10 portable colourimeter. To compare the colorimetric coordinates after the aging, of not protected and protected with graphene samples, we have calculated a protection factor (PF), according to:

$$PF(\%) = \frac{\Delta E^*_{\text{colour without graphene}} - \Delta E^*_{\text{colour with graphene}}}{\Delta E^*_{\text{colour without graphene}}} \times 100 \quad (2)$$

Details about the aging of the mockups are reported below. The error related to ΔE^* values obtained using this instrument is ±0.5.

Specimens were artificially aged under UV and visible lighting to induce the fading of the dyes and the paints. A device emitting UV light of a λ = 254 nm, power intensity equal to 4–6 mW, and, a panel of lamps emitting white/visible light with a power intensity of 33 mW and average temperature of ~50 °C, were used to

 This journal is © The Royal Society of Chemistry 2023

Open Access Article. Published on 23 February 2023. Downloaded on 8/16/2024 2:06:04 PM.
This article is licensed under a Creative Commons Attribution-NonCommercial 3.0 Unported Licence.

monitor the degradation of the dyes and the paints. The accelerated aging for all specimens lasted from 24 to 390 hours. This accelerated aging time corresponds to an aging under real conditions equal to a time interval from ~30 years to ~100 years.[38,39] The exposure for the architectural paints can be considered as an equivalent for ~1 to 2 years of intense sun solar light.[38] A portion of the painted surface was covered during the aging, to be used as a reference. Periodically, reflectance spectra were acquired and the colorimetric coordinates were obtained as described previously.

For the reduction of GO after irradiation with Ultra-violet and visible light, a common microscopic glass was cleaned with oxygen plasma treatment for 2–3 minutes to remove any impurities from the surface and then it was dip-coated with aqueous solution of GO with a concentration of 3.2 mg ml^{-1}. The specimens were left to dry completely in dark nitrogen-filled chamber in order to avoid the reduction of the GO films prior to aging. The specimens were aged in UV light for 1 full day and under visible light for 7 full days. For the aging with UV light, intense UVC (254 nm) radiation was emitted by a device (8 W, 230 V) with 3 available UV lamps, one for 365 (UVA, longwave), one for 302 (UVB, midrange) and finally one for 254 nm (UVC, shortwave). The spectrum for the UV-C lamp of the device, shown in Fig. S1,† was acquired using a LI-1800 portable spectroradiometer. Several measurements for varying distance between the spectroradiometer and the device were taken (Table S1†). The power coming from the UVC lamp of the device was measured with a thermal power sensor (THORLABS PM100A, sensor: S322C) while the diameter of the sensor was of 25 mm. Since the UVC lamp of the device is on and applied exactly above the examined specimen (distance equal to 2–3 cm, Table S1†), a temperature equal to 30–32 °C is induced. For the aging with visible/white light, an in-house built aging chamber, equipped with seven lights panel emitting white/visible light was exploited. The already presented spectrophotometer was used for obtaining the relevant spectrum of the panel emitting visible light. The panel shows a power intensity of 3 mW and induces an average temperature of ~50 °C to the under-lighting surface, which holds a distance of 5 cm from the light source. The power coming from the panel (with all seven lamps on) was measured with the same before-mentioned thermal power sensor.

Atomic Force Microscopy (AFM) images were collected in peak-force tapping mode (Bruker, Dimension-Icon), by using ScanAsyst-Air probes (silicon tips on silicon nitride cantilever, Bruker) with 0.4 N m^{-1} nominal spring constant of the cantilever. The electrical resistance (conductivity) measurements were performed by using a Keithley 2420 source meter unit (SMU) in a four-probe configuration with a specimen dimension of 15 × 15 mm^2 and an average film thickness of 270 μm.[40,41]

Results and discussion

Effective liquid-phase exfoliation of graphene and other 2D materials for the preparation of enhanced colours

In order to fully exploit the potential of graphene and other 2D materials, a preliminary optimization of the liquid exfoliation process has been conducted. Actually, the commercial graphene powder consists of graphite nanosheets, as revealed by optical microscopy and Raman spectroscopy (Fig. 1A and B, and Fig. S2†). In fact, the characteristic asymmetric shape of the 2D peak suggests that the nanosheets are composed of more than 10 graphene layers.[42] The G peak position appears at 1580 cm^{-1} whereas the D peak is very weak, revealing lack of crystal edges and structural defects, which is expected for the relatively large graphite flakes employed here. *N*-Methyl-2-pyrrolidone (NMP) is one of the most commonly adopted solvents for the efficient exfoliation of graphene and transition-metal dichalcogenides,[43] due to its values of surface tension and Hansen solubility parameters that well match with those of graphite and other layered materials.[44] Nevertheless, NMP has been recently classified as a substance of very high concern.[45] In this study, we managed to achieve a good exfoliation by using a binary mixture of water–ethanol as solvent, which is not only a much safer alternative than NMP[46] but it is also pivotal for successful mixing of artistic or architectural paints. To do so, the composition of the ethanol-in-water solution was

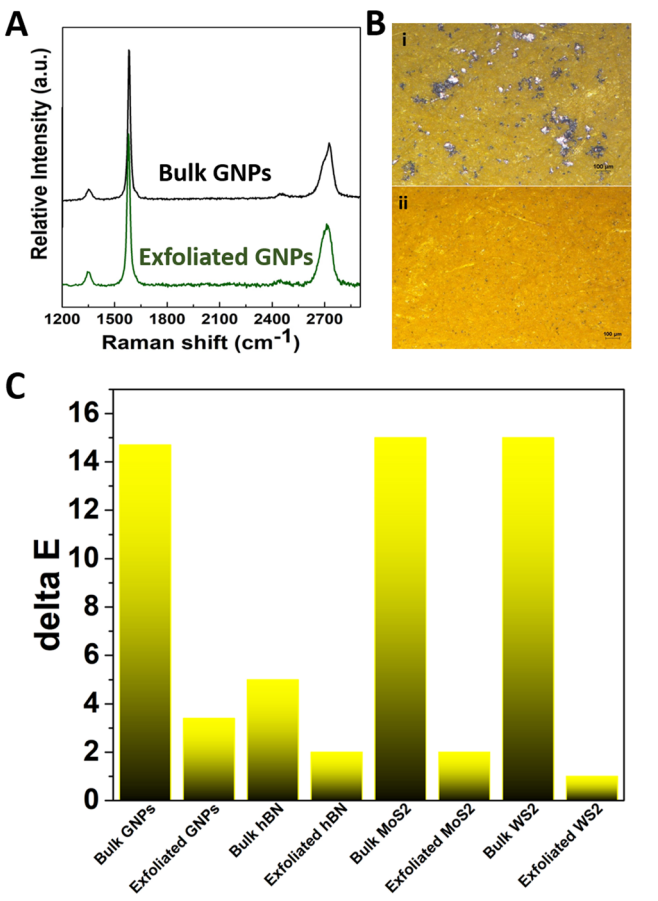

Fig. 1 Doping colours with graphene nanoplatelets and 2D materials using liquid phase exfoliation. (A) Representative Raman spectra of GNPs before and after LPE in water/ethanol. (B) Optical microscopy images of paper mockups dyed with tartrazine doped with GNPs as received (i) and after LPE (ii). (C) The colorimetric index ΔE^* for tartrazine doped with graphene, hBN, WS_2 and MoS_2 as received and after LPE.

Open Access Article. Published on 23 February 2023. Downloaded on 8/16/2024 2:06:04 PM.
This article is licensed under a Creative Commons Attribution-NonCommercial 3.0 Unported Licence.

fine-tuned in order to obtain a surface tension that matches the corresponding value of NMP.[47,48] The optimized molar fraction of ethanol was estimated to be equal to 0.06 (Fig. S3†). The successful exfoliation of the graphitic nanopowder using the water–ethanol solvent has been therefore achieved, as demonstrated by optical microscopy and Raman spectroscopy (Fig. 1A and B) in which the three characteristic peaks D, G and 2D of graphene are clearly shown. As already known, the 2D peak is sensitive to the number of graphene layers since the resonant Raman mechanism is closely connected to the details of the electronic band structure[49] and this structure changes with the number and orientation of layers.[50] By focusing particularly on the 2D peak the Raman spectra of graphene powder before and after exfoliation (Fig. 1A), a transition from graphite to few-layer graphene is clearly observed, after the exfoliation process. In fact, a significant change in the shape of the 2D peak and an increase of the intensity ratio of the 2D to G peak can be observed when moving from graphite to graphene.[42,51] The successful exfoliation is also revealed in the comparison of optical microscopy images acquired from the powder before and after the exfoliation process.

In order to assess the optical properties of the produced graphene in water/ethanol dispersions for possible application into commercial inks/paints, UV-vis spectroscopy was employed (part of the '*Mechanism of protection*' shown on Fig. 6B). It is interesting to note that the produced graphene dispersion shows the characteristic peak of graphene located at 280 nm, in agreement with other studies,[52] suggesting the maintenance of the sp^2 carbon structure during the dispersion process. The intensity of this peak increases as the concentration of the graphene is increased in the water/ethanol dispersion. Also, the absorbance is quite high for the whole spectrum for relatively low graphene concentrations. It is worth noting, that the ability for absorbing visible light can also assist in the protection of inks/paints from degradation[2] as will be presented further below. The as-resultant semi-transparent dispersions combine high rates of visible absorbance without paying the analogous expenses in their optical appearance, thus leading afterwards to acceptable colour hues. On the other hand, GO is known to be hydrophilic and can be incorporated easier into water-based inks and paints. The absorbance spectra of aqueous solutions of various GO content are shown in Fig. S4,† from which the characteristic peak attributed to graphene at the UV range is confirmed. These findings are in accordance with relative publications for GO dispersions in water.[52] The corresponding wavelength of the peak is located at 234 nm.

It is attributed to C–C bonds of the π to π^* transition, while a shoulder peak at 270 nm due to n to π^* transition of the C=O bonds of the carbonyl and carboxylic groups located in the GO lattice is also observed.[53] An important observation is that GO shows a proportional increase of the intensity as the concentration of graphene is increased. Also, it is worth mentioning that when the GO concentration is raised from 0.1% w/w to 1% w/w, the maximum absorbance reaches a maximum value of 0.8. Then, a significant and sharp decrease of the absorbance is obtained in the visible region.

In a similar approach to that applied for the exfoliation of GNPs, successful exfoliation of hBN, WS_2 and MoS_2 has also been achieved in water/ethanol mixtures (Fig. S5†). In particular, for the case of WS_2 the molar fraction of ethanol in the mixture was determined in order to achieve a surface tension that matches the corresponding value for NMP (*i.e.* 0.06); while for the cases of MoS_2 and hBN, it was determined on the basis of the surface tension of Benzyl Benzoate.[47,48] For the latter, the mole fraction of ethanol-in-water solution that was employed was equal 0.04. As shown in Fig. S6–S8,† the optical microscopy images of all the examined materials reveal an important reduction in the size of the crystals after the exfoliation, while from Raman spectra, it can be also deduced that a transition from multi-layered to few-layered materials is achieved.[54,55] Again, UV-vis absorption spectra indicate the presence of absorption in the UV regions which are of interest for application related to colour protection. The characteristic absorbance peaks of hBN in the UV-region are clearly detectable at 207 nm and, for higher hBN content, a peak at 238 nm. Also, the intensity of the peaks is increased as the hBN concentration in the solution is increased.[56] By observing the absorbance spectra of the prepared MoS_2 solutions (as the baseline solution was measured an ethanol/water mixture with mole fraction of ethanol equal to 0.04 and subtracted at the presented spectra), several characteristic absorbance peaks in the visible region are detectable (667 nm, 480 nm, 420 nm), as well clear UV absorbance is evident (209 nm and 230 nm). The intensity of the peaks gets higher for higher MoS_2 content in the solution.[57] From the absorbance spectra of the prepared WS_2 solutions (as the baseline solution was measured an ethanol/water mixture with mole fraction of ethanol equal to 0.06) that were acquired, several characteristic absorbance peaks of WS_2 in the visible region are present (650 nm, 470 nm, 420 nm), as well as a clear UV absorbance is evident (202 nm, 248 nm and 335 nm). The absorbance spectra are shifted upwards for higher WS_2 content, which means that more visible and UV light of particular wavelengths is absorbed.[57] Dispersions of graphene and other 2DMs in non-toxic solvents can be easily added into colours, inks and paints, as described in the Experimental section and shown on Fig. S3.† Actually, since it is known that each layer of graphene absorbs 2.3% of visible light,[14] we first assessed if the presence of the nanomaterial could affect significantly the visual appearance of the colours. Very interestingly, by using the proposed shear mixing route in water/ethanol, the presence of graphene and other 2DMs is not found to affect significantly the visual appearance of the colour. In fact, as demonstrated in the case of the yellow azo dye tartrazine, the colour is homogeneous and remains mostly unaltered, with colour difference index ΔE^* lower than 3 (Fig. 1C and S9†). We want to underline that in this investigation, we chose the worst-case scenario of a light colour (*i.e.* yellow).

As shown in a previous work,[29] the presence of graphene monolayer coatings on paintings can be only perceptible

 This journal is © The Royal Society of Chemistry 2023

Open Access Article. Published on 23 February 2023. Downloaded on 8/16/2024 2:06:04 PM.
This article is licensed under a Creative Commons Attribution-NonCommercial 3.0 Unported Licence.

under very close inspection when deposited on dark colours (such as blue), whereas it is perceptible at a glance when deposited on light colours (such as pink or yellow). Optical microscopy images of paper specimens dyed with graphene-doped and 2DMs-doped tartrazine do not show any aggregate or darkening spots. On the contrary, direct ultrasonic sonication of graphite or other 2DMs powder into tartrazine/water solution has been found to lead to significant darkening of the colour, quantified by a ΔE^* index of ~15, with macroscopic black spots, probably from remaining bulk material, due to unsuccessful exfoliation and formation of aggregates of dimensions 10–100 μm. Therefore, this demonstrates that the employed liquid exfoliation route can lead to the production of dyes enhanced with well-dispersed graphene and other 2DMs. The better exfoliation and homogeneous incorporation of graphene by using the proposed method has been demonstrated also for paints for artistic purposes, such as acrylic and architectural paints (Fig. S9†), the ΔE^* index being significantly lower than those prepared by direct ultrasonic sonication (encoded as "bulk").

GRMs and 2DMs prevent the degradation of colours

In order to investigate the effect of GRMs and other 2DMs on the fading of colours, a commercial ultramarine ink was investigated as proof of concept. Actually, this colour undergoes degradation phenomena upon exposure to light and its failure in historic, as well as, modern paintings has been reported several times in the literature and is often referred to as "ultramarine disease" or "ultramarine sickness".[58] In fact, as demonstrated by UV-vis absorption spectroscopy, the characteristic peaks of ultramarine ink significantly decrease upon exposure to light (Fig. 2A). Very interestingly, the addition of GNPs is found to mitigate this effect and is therefore expected to prevent the fading of the ink to a certain extent. Therefore, paper mock-ups were painted with ultramarine ink added with GNPs and were artificially aged under different lighting conditions (*i.e.* UV and visible light) and the colorimetric differences were monitored. For instance, Fig. 2B shows representative pictures of specimens coloured with ultramarine ink with different amount of GNPs (0.1% w/w, 0.3% w/w) upon exposure to UV-C light for 5 days and upon exposure to visible light for 36 days. In both cases, it can be observed that the colour of the reference specimen has faded significantly, which indicates that it has undergone considerable degradation compared to the samples containing graphene. This is confirmed by the fact that the colour difference between the part of the aged specimen in relation to the covered area that was not irradiated and retained its original colour, is more pronounced in the case of the control specimen, less pronounced in the case of the 0.1% w/w GNPs and almost negligible in the case of the 0.3% w/w GNPs specimens.

To compare the colorimetric coordinates after aging of control samples *versus* those coloured with GNPs-enhanced inks/paints, we have used the protection factor (PF), as defined in eqn (2). GNPs, for accelerated aging under the influence of UV-C, showed a protection factor of 12.4% for 0.1% w/w and 22.6% for 0.3% w/w GNPs, respectively (Fig. 2B). For visible light, the corresponding protection factors were 12.8% for 0.1% w/w and 21.9% for 0.3% w/w graphene, respectively. It can be concluded that as the GNPs concentration increases, the ΔE^* index drops and this results in higher protection factors.

The addition of GO to the same ultramarine ink has been found to be effective against ultramarine degradation, as well. The absorbance spectra of doped inks with 0.25, 0.5 and 1% w/w GO before and after aging with UV light are presented in Fig. 3A and S10.† As shown, there is a clear increase of absorbance over the whole spectral range as a result of GO addition. Also, as expected, the 1% w/w GO-based solution exhibits the higher absorbance out of the three concentrations tested here. Furthermore, it is evident that the increase of absorbance within the visible range is not as high as in the UV range, therefore the corresponding transmittance should be relatively high as desirable for a practical application. From Fig. 3A and S10,† it is deduced that an important decrease of the characteristic peak is observed after the aging, while the addition of GO mitigates this decrease. The more GO in the solution the lower peak intensity difference between the blue colour before the aging and the graphene-based ink after the aging. This can be considered as a proof for the protection of this dye. Furthermore, the width of the characteristic peak is not significantly affected neither by the GO addition nor by the aging. GO is believed to be responsible for an important increase of the UV absorbance and a moderate increase of the visible absorbance, something that implies a moderate decrease of visible transmittance.

Fig. 3 shows representative Pelikan Ultramarine specimens after accelerated aging for 3 hours under UV-C radiation. It is observed that the reference sample is more discoloured compared to the sample containing GO. Also, the specimen with a GO content of 0.03% w/w seems to have retained its colour to a greater extent compared to the sample with a GO content of 0.015% w/w. The protection of GO against degradation for the ultramarine sample is shown in Fig. 3. Finally, for accelerated aging under the influence of UV-C, the presence of GO provided a protection factor of 5.3% for a content of 0.015% w/w and 13.6% for a content of 0.03% w/w. It was rational to find the limitations of the GO content that can be incorporated into the blue ink without altering unacceptably the colour hue. For example, in Fig. 3B it is shown a filter paper coloured with blue ink/GO 0.1% w/w solution, and comparing this specimen with the reference, it shows a ΔE^* equal to 5.8, which is relatively high. After performing accelerated aging of this sample using UV light, the exposed blue area got darker because the GO reduction (as is fully explained further below) resulted in a ΔE of 30.7, which is unacceptably high. After performing a colorimetric study with varying GO contents, it was decided to prepare samples with very low GO content, as low as 0.015% and 0.03% w/w. The effectiveness of graphene and of GO against colour fading has been demonstrated also for other colours (*e.g.*, yellow and pink, see Fig. S11†), reaching protector factor as high as 43%. Such high rates of protection can endow to the as-formulated colours additional years of lifetime (since

Open Access Article. Published on 23 February 2023. Downloaded on 8/16/2024 2:06:04 PM.
This article is licensed under a Creative Commons Attribution-NonCommercial 3.0 Unported Licence.

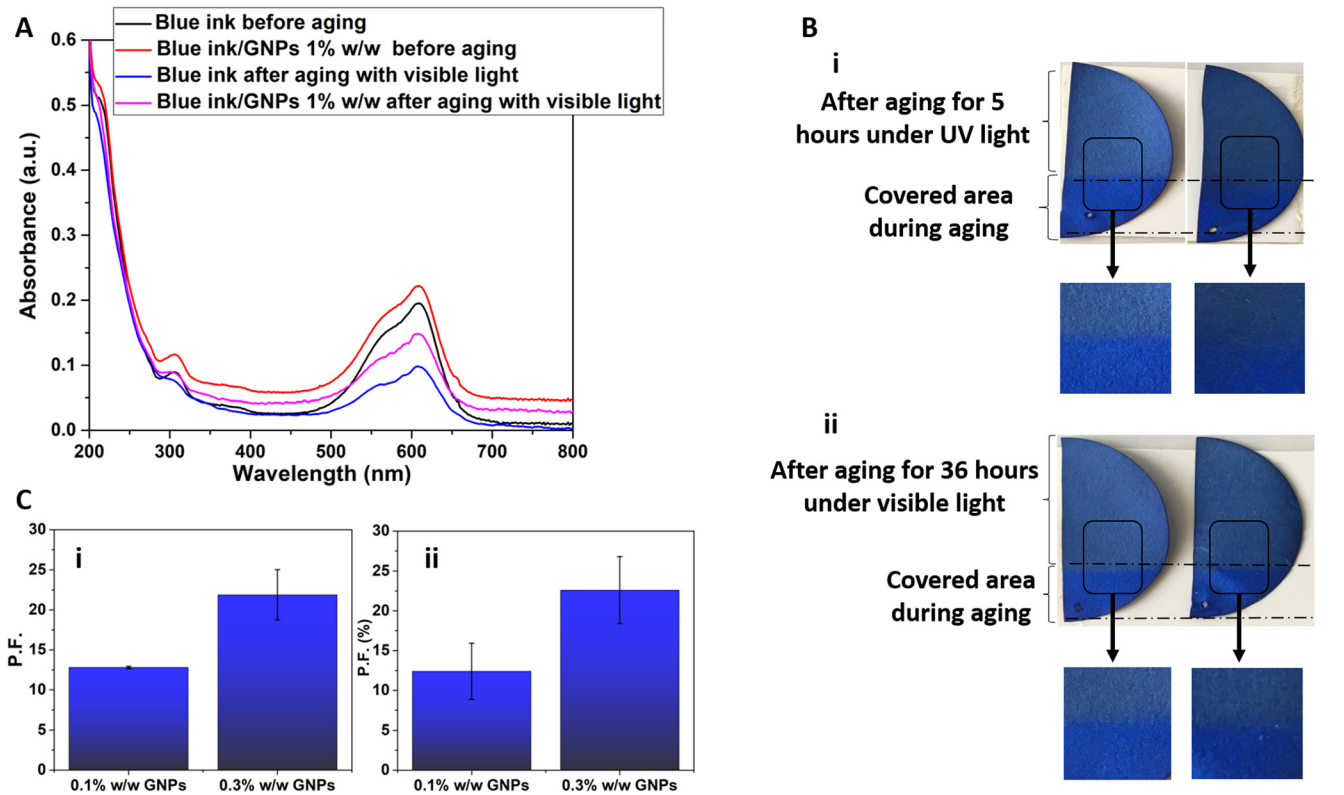

Fig. 2 Graphene nanoplatelets prevent the fading of ultramarine ink. UV-vis absorption spectrum of ultramarine ink, with and without graphene, before and after irradiation to visible light for 80 hours (A). Representative images of mock-ups coloured with ultramarine ink without and with GNPs, after 5 days of accelerated aging with UVC radiation and 36 days with visible light (B). Protection factors different mock-ups upon ageing with UV (C) (i) and visible light (C) (ii) as a function of graphene content.

their accelerated ageing is intense and stands for ~30 to 100 years).

Samples dyed with the commercial ultramarine ink doped with WS_2, MoS_2 and hBN after their exfoliation were examined through accelerated aging by irradiating them with UV and visible light for 5 hours in both cases. Protection factors are plotted in Fig. 4, and from those it can be concluded that WS_2 seems to perform better than the other two 2DMs both for aging with UV and visible light. In contrast, hBN shows to induce the lowest fading resistance while an intermediate behaviour is observed for MoS_2.

GNPs boost further multi-functionalities into paints

GNPs and GO were added to water-soluble commercial architectural paints, and aging tests were performed inside an environmental chamber in order to reproduce the effects of combined temperature, relative humidity and UV light.[59,60] Actually, the GNPs seem to assist the paint to behold the colour hue and lightness. In fact, the sample with 0.1% GNPs exhibits a protection factor of 23% when compared to the bare substrate, after three weeks of continuous aging inside the chamber. Furthermore, as revealed by optical microscopy in Fig. 5, the presence of graphene and GO prevents the formation of micro-cracks and micro-failures which are present in the bare paint after aging.

Another interesting feature is that the addition of only 0.1% w/w GO dispersion into a commercial red water-soluble architectural paint is enough to decrease the electrical resistance by two orders of magnitude, as shown in Table 1. Consequently, an increase in electrical conductivity is achieved, demonstrating the multi-functionality that these novel paints can show. This means that the GO-doped paint can be exploited as electrostatic discharge coating, since its behaviour shows a transition from insulator to dissipative. This is quite important since a paint with an anti-static behaviour creates a preferred pathway for the flow of electricity, keeping the electrical charge under control as the charge is drained. The charge flows over the surface and into a grounding point and then vanishes. GO is known to be non-conductive due to the absence of percolating pathways between sp^2 carbonaceous clusters which is actually at the base of the carrier transport mechanism in graphene. A mono-layered GO consists of a hexagonal carbon network having both sp^2- and sp^3-hybridised atoms of carbon, carrying hydroxyl and epoxide functional groups on either side of the layer, while the layer edges are mainly occupied by carboxyl and carbonyl groups.[61] In that way, the functional groups attached to the plane affect the conductivity, while the corresponding ones attached to the edge may not. In contrast, GO as a bulk material has large chemical functional groups attached to the carbon plane that show structural defects

 This journal is © The Royal Society of Chemistry 2023

Open Access Article. Published on 23 February 2023. Downloaded on 8/16/2024 2:06:04 PM.
This article is licensed under a Creative Commons Attribution-NonCommercial 3.0 Unported Licence.

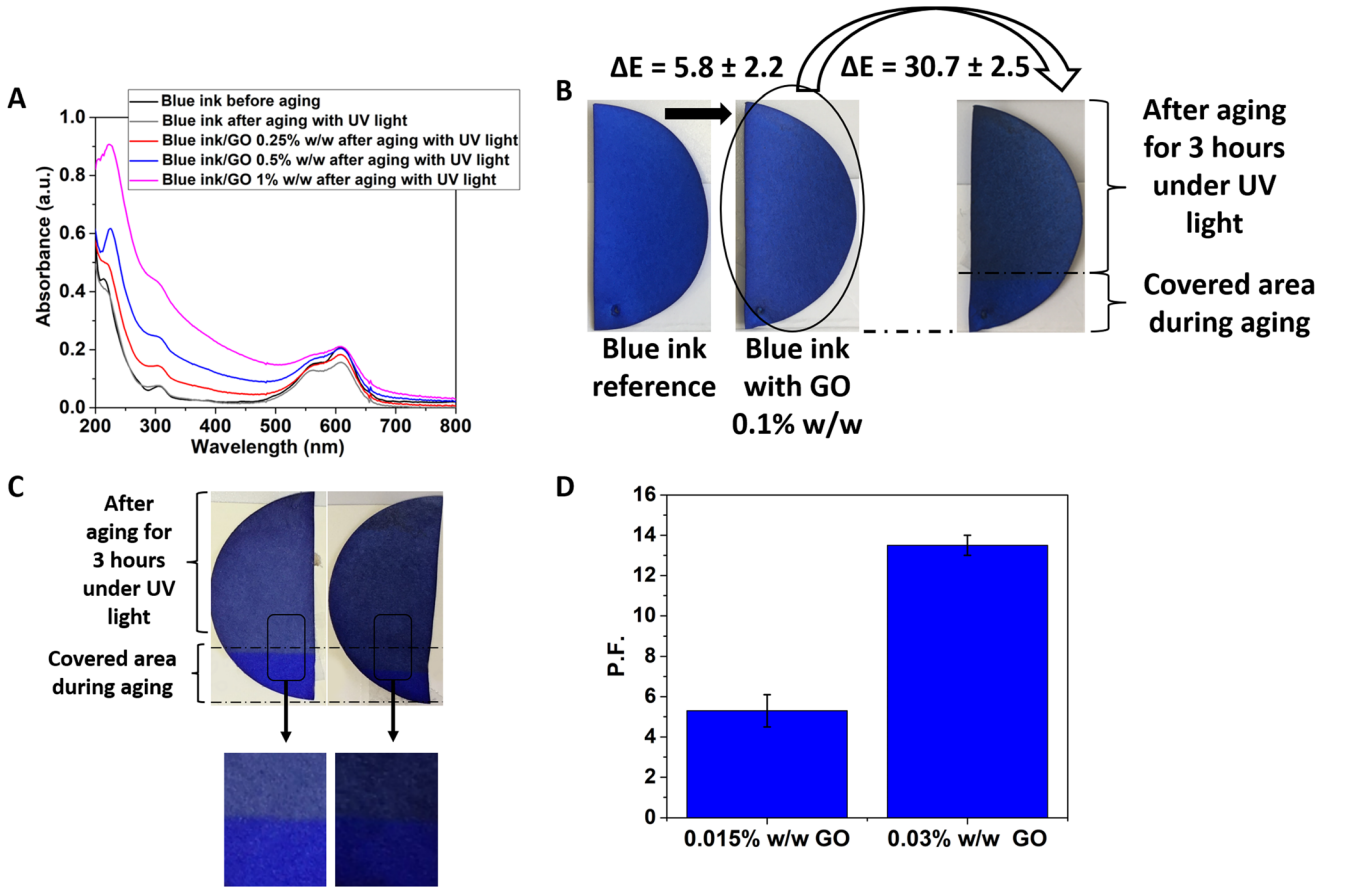

Fig. 3 Graphene oxide prevents the fading of ultramarine ink. UV-vis absorption spectrum of ultramarine ink, with and without graphene oxide, before and after irradiation to UV light (A). Filter paper coloured with blue ink reference and with GO 0.1% w/w, before and after aging with UV light (B). Filter papers dyed with blue ink (from left to right), a reference sample and a sample with 0.03% w/w GO after aging with UV light (C). Protection factor for GO content equal to 0.015% w/w and 0.03% w/w in blue ink after accelerated aging upon exposure to UV light (D).

within the plane, which can strongly lower the electrical conductivity. Nevertheless, the conductivity can be restored by attaching polymers or polymerization initiators onto the GO platelets which can chemically reduce the oxidized surface.[61,62]

The mechanism of protection provided by GNPs and 2DMs and the 'smart paints'

In order to shed light on the mechanism of protection offered by graphene and other 2DMs against the fading of colours triggered by light in an environment with oxidative media, tartrazine was chosen as model system, as conducted previously in another work by our group.[29] In fact, tartrazine is known to undergo photolytic degradation upon UV and visible irradiation, which results from the azo bond cleavage and following rupture of its characteristic five-membered ring.[63] GNPs were added to a water solution of tartrazine (0.1% w/w GNPs into the sol) as described in the Experimental section. Cardboard specimens were dyed with tartrazine with and without GNPs, and were subjected to an accelerated aging with UVC radiation for 4 weeks. Even from the first week of the aging period, GNPs addition seems to protect the maintenance of the colour hue by lowering the decolourization rate. As shown previously for other colours, the ΔE^* index is found to decrease with exposure time and a protection factor equal to 37.7% ± 2.5 has been determined for the tartrazine doped with GNPs (Fig. S12 and S16†), suggesting that this specimen is more protected against the dye degradation. Raman spectra were collected from the tartrazine mock-ups and, as shown in Fig. 6A, after exposure to UV light for 7 days, the characteristic Raman peaks of tartrazine weaken, compared to the cardboard peak located at 1094 cm^{-1}, as a result of the decomposition of the dye. However, when the exfoliated GNPs are embedded into tartrazine, its Raman spectrum remains unaltered after exposure to UV light. This finding provides a spectroscopic proof of the effectiveness of GNPs against colour degradation, and has been confirmed also by UV-vis absorbance spectroscopy (Fig. S13† – MB UV vis). As shown earlier, the GNPs and the GO used for the needs of this study, show a broad peak from 200 to 350 nm (UVC, UVB and UVA for the GNPs), and, from 200 to 300 nm (UVC and UVB for the GO). However, the protection against dye photodegradation provided by GRMs is not only attributed to its capability of absorbing UV light (see

Open Access Article. Published on 23 February 2023. Downloaded on 8/16/2024 2:06:04 PM.
This article is licensed under a Creative Commons Attribution-NonCommercial 3.0 Unported Licence.

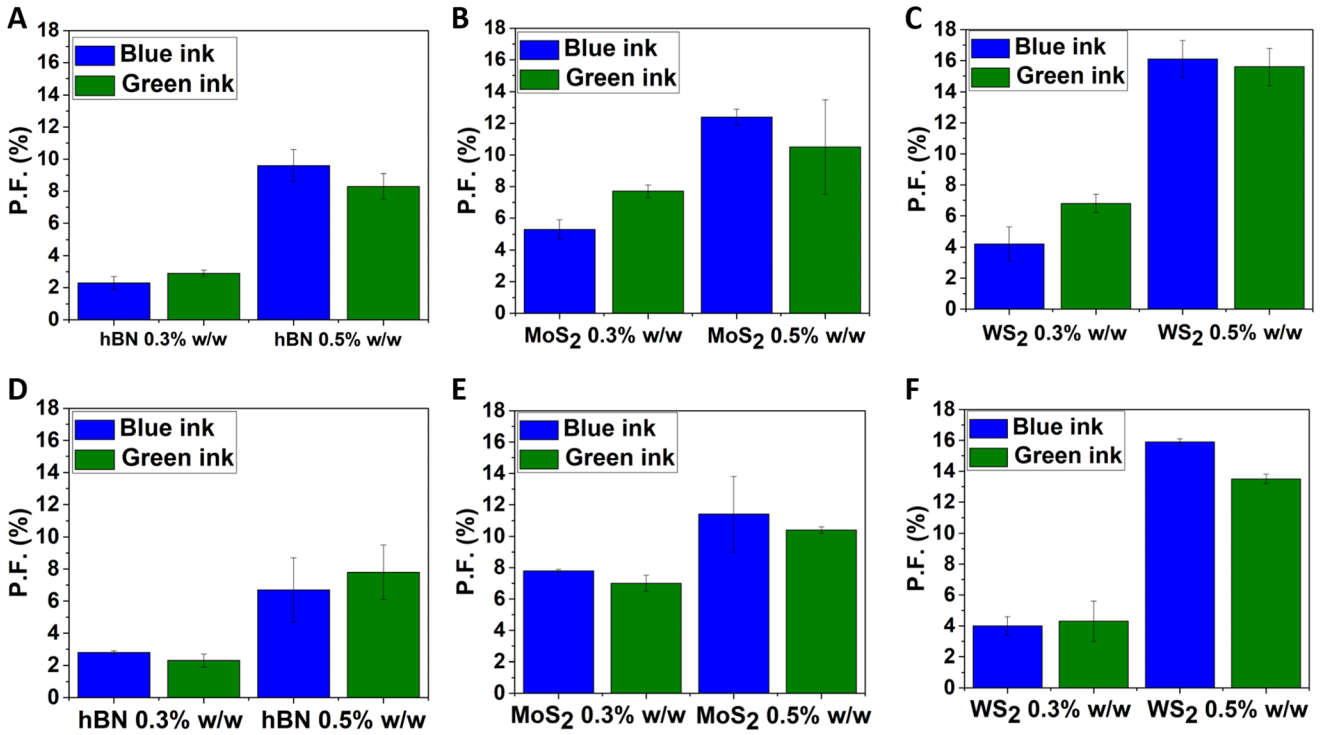

Fig. 4 Protection factors of filter papers coloured with blue and green inks, enhanced with hBN (A), MoS_2 (B), and WS_2 (C) after aging with UV light. (D–F) Protection factors of filter papers coloured with blue and green inks, enhanced with hBN (D), MoS_2 (E), and WS_2 (F) after aging with visible light.

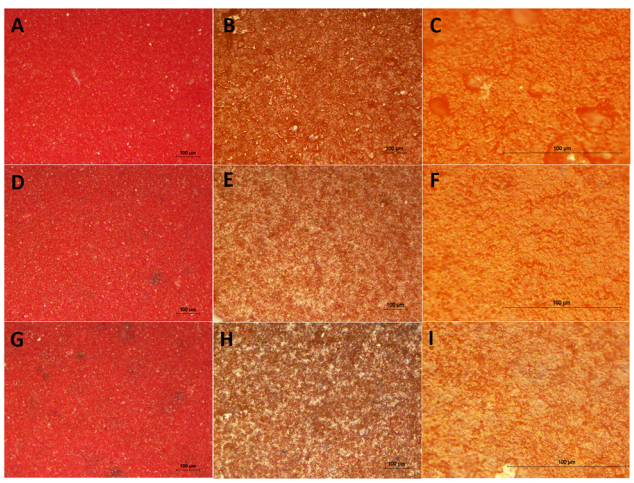

Fig. 5 Representative optical microscopy images of a red architectural paint. In the first row, a reference sample before the aging (A), and, after the aging (B and C). At the middle, the same red paint enriched with 0.1% GNPs before the aging (D), and after the aging (E and F). At the bottom, the same red paint with 0.1% GO added before the aging (G) and after the aging (H and I). All representative specimens had been exposed to an accelerated aging inside an environmental chamber.[59,60] Larger scale bars have been used for the photos (C, F and I) of the last column. On (B), small craters which are the initiator points for micro-cracking can be detected after the aging of the neat paint, while correspondingly on (E) and (H), GNPs seem to prevent the creation of such points.

Table 1 Electrical resistance of architectural paints. Specimens with fixed dimensions were tested

Examined sample	Resistance (MΩ)	Resistivity (Ω m)
Neat red architectural paint	13 000	3.510
Red architectural paint with GO dispersion 0.1% w/w	125	33

Fig. 6B), but also to the physical barrier function and ultra-high surface area for free radical scavenging.[64] For this reason, 2D nanomaterials like graphene have emerged as a new category of anti-oxidants. In fact, the chemical reactivities and protection ability of GNPs toward some model free radicals and reactive oxygen species (ROS) have been recently demonstrated.[64–66]

Actually, GNPs are able to protect the targets from oxidation while they are highly-efficient as hydroxyl-radical scavengers. Since a hydroxyl radical is created photolytically, the total anti-oxidation activity is a synergy of the preventive anti-oxidant function (resulting from the UV absorption) and $^{\bullet}OH$ radical scavenging (Fig. 6).[64] In this regard, it is interesting noting that Raman spectra collected from graphene-poor locations of the GNP-doped tartrazine sample show that, after aging, the characteristic peaks of tartrazine still remain unaltered.

This journal is © The Royal Society of Chemistry 2023

Open Access Article. Published on 23 February 2023. Downloaded on 8/16/2024 2:06:04 PM.
This article is licensed under a Creative Commons Attribution-NonCommercial 3.0 Unported Licence.

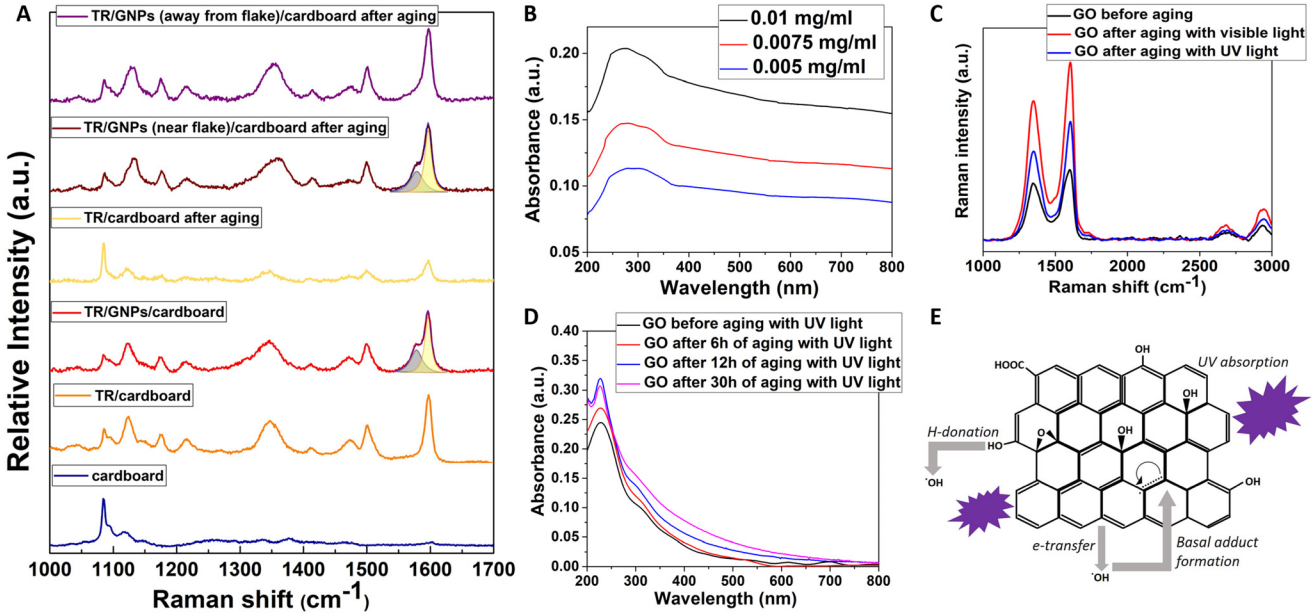

Fig. 6 Mechanism of protection. (A) Representative Raman spectra of cardboard, tartrazine (TR), tartrazine-coloured cardboard (TR/cardboard) before and after aging with UV light for 7 days, GNPs-doped tartrazine-coloured cardboard (TR/GNPs/cardboard) before and after aging with UV light for 7 days. Lorentzian fits (represented by the coloured peaks) are superimposed on the experimental data. (B) UV-Vis absorbance of GNPs solution (C) Raman spectra for representative GO, rGO specimens after irradiation with white/visible light for 7 days, and, rGO after irradiation with UV light for 1 day, respectively. (D) UV-VIS absorbance spectrum of GO solution before and after aging under UV irradiation. (E) The relevant antioxidant mechanisms (UV absorption, $^{\bullet}OH$ adduct formation on sp^2-carbon sites; electron transfer, and hydrogen donation). The scheme shows that the primary antioxidant activity for graphene-based materials is against $^{\bullet}OH$ and is related to pristine sp^2-carbonaceous areas. Hydrogen donation is limited by the low population of phenolic OH, which are located on edge and not on basal sites.

Few-layered graphene is actually more active than a monolayer GO, despite the fact that it shows lower surface area, something that denotes that the basic scavenging sites are connected with the sp^2-carbonaceous network rather than the oxygen-containing functional groups.[64] This can be explained as following: GO is a weak hydrogen donor, because of the non-phenolic nature of most OH groups on GO, that are located at basal sp^3-carbonaceous regions which do not favour radical resonance stabilization following hydrogen donation. The principle scavenging function is connected to pristine sp^2 carbon domains onto basal surfaces rather than hydrogen-donation from hydroxyl groups. The activity of oxygen-containing groups may be independent regarding pH, but the high activity of few-layered graphene relative to GO has been obtained for both pH = 3 and pH = 7 in distinct systems. The weak activity of GO as a donor anti-oxidant material is in consistency with its chemical structure. A lot of anti-oxidants are phenolic compounds whose radical forms following hydrogen-donation[67] get stabilized by resonance structures, in which the un-paired electron can be located onto the oxygen atom,[68] or else on *ortho* or *para* carbon atoms on the adjacent aromatic ring. GO consists of a lot of hydroxyls and shows extensive aromaticity in the form of pristine sp^2-carbon domains between the oxidized regions, but does not show high activity as a hydrogen-donor. Usually for the most accepted models regarding GO structure, the OH groups are placed out-of-plane at basal sites, while the oxidation of the C=C double bonds has generated sp^3 local sites which do not render the adjacent bonded structure capable of radical resonant stabilization. These basal OH groups on GO do not lead to high anti-oxidation activity. Consequently, the basic radical scavenging sites seem to be connected to the pristine sp^2-carbon domains, that function through adduct formation[69] or electron transfer, as depicted in Fig. 6. For experiments involving UV-induced $^{\bullet}OH$ generation, the protection result is a synergy of UV absorption and radical scavenging by graphene.

For the case of the other 2DMs, the protection ability can be only secondarily ascribed to the different UV absorption spectra which are depicted in Fig. S6C, S7C and S8C.† Based on their UV-visible absorbance spectra, it is obvious that all three of them absorb UV light but in different wavelengths. MoS_2 and hBN have a clear absorbance peak at 230 nm, while WS_2 absorbs at 248 nm. This parameter should make a difference in their preventive antioxidant function since the accelerated aging was performed by using UVC light (250 nm). According to the protection factors for aging with UV light, indeed, WS_2 showed the highest protection. At the same time, comparing the protection ability of MoS_2 and hBN against fading upon exposure to UV light, there is a huge difference in the numbers, which means that the UV absorbance of the 2D materials cannot be considered the only property responsible for their protective effect. This statement can also be verified by the fact that both transition-metal dichalcogenides have similar absorbance spectra of visible light, yet the tungsten

Open Access Article. Published on 23 February 2023. Downloaded on 8/16/2024 2:06:04 PM.
This article is licensed under a Creative Commons Attribution-NonCommercial 3.0 Unported Licence.

disulphide exhibited a higher anti-fading effect. In the case of hBN, it does not absorb in the visible region and consequently has the lowest protection ability in the accelerated aging experiments with visible light. A crucial observation from the PF plots (Fig. 4) is the fact that none of the 2D materials seems to be affected by the type of light used for aging, and as a result, the calculated PFs are similar for aging with UV and visible light, for each material. Thus, it can be concluded that the light absorbance of each material, particularly at the wavelength of the light that is used for aging, affects the protection ability of the 2D materials; however, it is not the dominant property for their anti-fading result. From a literature review about the anticorrosion and antioxidant applications of 2D materials, several publications can be found reporting the incorporation of flakes of 2D materials, produced mainly by the LPE method like the one used in this work, in polymer matrices to enhance their mechanical, thermal and chemical stability. The most appealing property of hBN is its superior chemical inertness. According to literature, only the edges of hBN can become chemically active, and only the electrophilic boron atoms of these edges can form covalent bonds with OH– radicals.[70,71] At the same time, the in-plane bonds of hBN are very strong, which means that hBN sheets in few-layers flakes are less prone to breakage during the exfoliation, and fewer edges are created.[72,73] As for the transition-metal dichalcogenides, there are several references about their gas barrier properties, antibacterial and thermal resistance ability.[74,75] Because these materials do not have such stable structure as GNPs and hBN, flakes with more edges are created during their exfoliation.[76,77] Mostly monolayers but also few-layered, can absorb humidity and oxygen species at edges and vacancies of their structures.[78] The transition-metal dichalcogenides protect the dye by trapping ROS and corrosive gases in their structure, eliminating thus the degradation reactions that occur on the surface of the dye. Summarizing all the above, the other 2D materials show less anti-fading effect than GRMs because, despite their undoubtful UV light absorbance properties, they either remain chemical inactive and cannot prevent the degradation reactions (hBN) or the ROS trapping ability is not so sufficient (MoS_2, WS_2). All the scientific evidence indicates that the highest protection effect of GNPs can be attributed to the balance of the radical scavenging ability while retaining their chemical inertness in combination with light absorbance.

GNPs demonstrate OH radical scavenging properties inversely proportional to their total surface area according to the following order FLG > rGO > GO.[64] However, in our experiments, we note that GO-doped colours present a protection factor comparable with GNPs, despite GO content is one order of magnitude lower. In order to clarify this aspect, we should recall here that it has been demonstrated that GO can be reduced in water by UV light.[27,28] We also examined a possible reduction of GO using white/visible irradiation and UV irradiation as well. In these experiments (Fig. S14†), GO had not been added inside some ink but only diluted to deionized water. From Fig. 6, the Raman spectra of such sample after irradiation clearly indicate the reduction of GO but each irradiation leads to different degree of reduction. It is evident that for the starting material, the characteristic D- and G-peaks are present, respectively, at 1355 and 1584 cm^{-1} with a D/G intensity ratio of 0.85. After irradiation, the spectra exhibit a slightly shifted G-band peak towards higher wavenumbers and D/G intensity ratios of 0.78 and 0.76, for the reduction with visible and UV light, correspondingly. This can be ascribed to the graphitization of the prepared sample, as already reported in the literature,[79] and additionally, implies that the residual stress/strain before and after the reduction remains unaltered.[80] However, the D/G intensity is highly dependent on the exact composition of the starting GO and the method through which the reduction process is obtained.[81] One of the key parameters affecting the efficiency of the reduction of GO is the total energy transmitted by the light ray to the sample, which is in fact required to break the C–O, C═O bonds. The energy absorbed by the sample or the absorption rate of the light is another factor contributing to the reduction of GO. Based on the absorbance of untreated GO solution, GO light absorption is optimum at wavelength about 234 nm. The UV wavelength is about 254 nm, which is near to the optimum absorption wavelength for GO while for the white/visible light, a distribution of the absorption is obtained across these wavelengths. However, it seems that the reduction observed with UV light is less intense compared to white/visible light, since the intensity of G and 2D peaks of the former is less prominent than the latter. It is assumed that the influence of the temperature (55 °C) attributed to the white/visible light applied on the GO causes its further reduction. From Fig. 6, it is observed that GO, before and after aging with UV light, exhibits an absorption peak at 235 nm – that corresponds to $\pi \rightarrow \pi^*$ electronic transitions due to the C═C bonds of GO – and a shoulder at ~300 nm – corresponding to $n \rightarrow \pi^*$ electronic transitions due to the C═O bonds of the carbonyl and carboxylic groups located in the GO lattice, exactly as reported in literature.[53] As the exposure time increases, the intensity of the absorption peak increases and this can be ascribed to GO reduction, the sp^2 hybridization being restored and the perfect graphene structure being approached. Fig. S14† shows the diluted GO before treated with UV and visible radiation. After the GO solutions were treated with UV for 160 hours, their optical appearance was changed from almost transparent to slightly brown. A similar effect can be observed for samples irradiated with white/visible light for 60 hours. The appearance changes slightly to bright brown especially for concentration solution 0.5 and 1%, but with a simultaneous formation of dispersed particles inside the solution.

For incident UV irradiation, a photoinduced chain reaction seems to be responsible for the reduction of GO.[79] The reaction is initiated using ultraviolet radiation that photo-ionizes the solvent which is water/ethanol binary mixture, releasing solvated electrons, which trigger the reduction. GO is transformed into rGO after the capture of the solvated electrons generated by ultraviolet photoionization of the solvent.[79] This reaction has been linked to the non-thermal nature of the

 This journal is © The Royal Society of Chemistry 2023

Open Access Article. Published on 23 February 2023. Downloaded on 8/16/2024 2:06:04 PM.
This article is licensed under a Creative Commons Attribution-NonCommercial 3.0 Unported Licence.

chemical reduction in that it is the chemical potential of the solvated electrons[79] that initiates the reduction instead of heating effects on barrier crossing. On the other hand, the reduction of GO *via* visible light[82] and heating it[83] is already known and well-presented. The *in situ* chemical reduction that occurs when the GO-doped ink or paint is exposed to UV or visible light, implies that the content of graphene-like structure increases with the exposure time. This does increase the resistance against fading of the colour, thus giving a 'smart' feature to the ink/paint itself.

The synergy of UV and visible absorption, which, in turn, can lead to a larger number of graphene-like structures with time (in case of the reduction of GO), radical scavenging, elasticity and high surface area render GNPs appropriate for targeted anti-oxidation applications as dispersed fillers, or as agents which reduce the production of ROS.

Conclusions

In this work the protecting ability of graphene and other two-dimensional materials against the fading of inks and paints used in art and in architectural/buildings is presented. First of all, a green route for the liquid-phase exfoliation of graphene and other 2D materials using a water-based solvent is implemented. The successful dispersion of well-exfoliated nanomaterial has been achieved in dyes and commercial inks and paints, without significant changes of the visual appearance of the colours. Graphene-related materials (few-layer graphene and graphene oxide) and other 2D materials (hBN, WS_2 and MoS_2) have been found to protect several dyes and inks, with a maximum protecting factor of *ca.* 40%. GNPs were added also to architectural paints, which were subjected to a specific aging protocol combining the effects of temperature, humidity and UV radiation. Graphene was found not only to protect the colour of the paint with a protection factor of 23%, but also to prevent the formation of morphological defects on the surface of the paint. GO has been found to enhance the electrical conductivity of the architectural paints, fostering an anti-static behaviour which underlines the multi-functionality of such developed paints. Raman spectroscopy and UV-vis spectroscopy were adopted to investigate the mechanism of colour protection provided by GNPs, which is based on the synergy between UV absorption and the ability for radical scavenging of reactive oxygen species, for such materials. In particular, regarding the GO-doped colours, it was found that the intrinsic protection function is improved by the UV-assisted chemical reduction that occurs *in situ* during the aging of the paints. This phenomenon provides a smart feature to the GO-doped inks and paints, as the content of graphene-like structure increases with the ageing time. The proposed solution represents a feasible technology to get on the market in the close future; in fact, the green exfoliation/dispersion of the nanofiller is scalable and could be easily implemented within a typical production process of paints or varnishes based on mixing and dispersion steps. The convenient process and the tiny amount of nanofiller necessary to achieve good functionalities are not expected, therefore, to impact dramatically on the final cost of the 2DM-enhanced paint.

Author contributions

GG and MK designed the experiments, M.K. performed the experiments, MGPC, GP, GA, GT, AM, CP interpreted the data, and GG and MGPC drafted the manuscript. NK participated in the experiments of synthesising GO while C.G. conceived the work, participated in its design and coordination, supervised all experimental procedures and revised the manuscript.

Conflicts of interest

A patent application (No. PCT/EP2019/8167919) has been submitted to the European Patent Office (EPO) and another one has been submitted to the Hellenic Industrial Property Organisation (18/10/2021, Protocol No. 6026). The following authors are involved in the patents: M.K., G.G., M.G.P.C., G.A., G.P. and C.G. The remaining authors (A.M., C.P., N.K. and G.T.) declare no competing interests.

Acknowledgements

This work was funded by the European Research Council under the GraphenART Proof of Concept project (GA: 779985). The authors also acknowledge funding from the European Union's Horizon 2020 research and innovation programme under grant agreement Graphene Core 3 (GA: 881603) and from the European Commission for Horizon Europe under the research project GREENART (GA: 101060941).

References

1 K. Sterflinger and F. Pinzari, Minireview The revenge of time : fungal deterioration of cultural heritage with particular reference to books, paper and parchment, *Environ. Microbiol.*, 2012, **14**, 559–566, DOI: **10.1111/j.1462-2920.2011.02584.x**.

2 F. Vanmeert, G. Van Der Snickt and K. Janssens, Plumbonacrite Identified by X-ray Powder Diffraction Tomography as a Missing Link during Degradation of Red Lead in a Van Gogh Painting, *Angewandte*, 2015, 3607–3610, DOI: **10.1002/anie.201411691**.

3 G. van der Snickt, *et al.*, Combined use of Synchrotron Radiation Based Micro-XRF, Micro-XRD, Micro-XANES and Micro-FTIR for Revealing an Alternative Degradation Pathway of the Pigment Cadmium Yellow in a Painting by Van Gogh, *Anal. Chem.*, 2012, **84**(23), 10221–10228.

4 C. Jost, C. Muehlethaler and G. Massonnet, Forensic aspects of the weathering and ageing of spray paints, *Forensic Sci. Int.*, 2016, **258**, 32–40, DOI: **10.1016/j.forsciint.2015.11.001**.

Open Access Article. Published on 23 February 2023. Downloaded on 8/16/2024 2:06:04 PM.
This article is licensed under a Creative Commons Attribution-NonCommercial 3.0 Unported Licence.

5 T. Maggos, V. Binas, V. Siaperas, A. Terzopoulos, P. Panagopoulos and G. Kiriakidis, A Promising technological approach to improve indoor air quality, *Appl. Sci.*, 2019, **9**(22), 4837–4849, DOI: **10.3390/app9224837**.

6 M. Y. L. Chew, Design for maintainability of basements and wet areas, *Buildings*, 2021, **11**(2), 1–25, DOI: **10.3390/buildings11020075**.

7 K. S. Novoselov, *et al.*, Electric Field Effect in Atomically Thin Carbon Films, *Science*, 2004, **306**(5696), 666–669, DOI: **10.1126/science.1102896**.

8 S. Chen, *et al.*, Oxidation Resistance of Graphene- Coated Cu and Cu/Ni Alloy, *ACS Nano*, 2011, (2), 1321–1327.

9 R. Prasher, Graphene spreads the heat, *Science*, 2010, **328**(5975), 185–186, DOI: **10.1126/science.1188998**.

10 J. U. Lee, D. Yoon, H. Kim, S. W. Lee and H. Cheong, Thermal conductivity of suspended pristine graphene measured by Raman spectroscopy, *Phys. Rev. B: Condens. Matter Mater. Phys.*, 2011, **83**(8), 1–4, DOI: **10.1103/PhysRevB.83.081419**.

11 X. Li, W. C. H. Choy, X. Ren, D. Zhang and H. Lu, Highly intensified surface enhanced raman scattering by using monolayer graphene as the nanospacer of metal film-metal nanoparticle coupling system, *Adv. Funct. Mater.*, 2014, **24**(21), 3114–3122, DOI: **10.1002/adfm.201303384**.

12 X. Li, *et al.*, Unique Seamlessly Bonded CNT@Graphene Hybrid Nanostructure Introduced in an Interlayer for Efficient and Stable Perovskite Solar Cells, *Adv. Funct. Mater.*, 2018, **28**(32), 1–12, DOI: **10.1002/adfm.201800475**.

13 S. Chortarea, *et al.*, Hazard assessment of abraded thermoplastic composites reinforced with reduced graphene oxide, *J. Hazard. Mater.*, 2022, **435**, 129053–129077, DOI: **10.1016/j.jhazmat.2022.129053**.

14 R. R. Nair, *et al.*, Fine structure constant defines visual transparency of graphene, *Science*, 2008, **320**(5881), 1308, DOI: **10.1126/science.1156965**.

15 K. F. Mak, L. Ju, F. Wang and T. F. Heinz, Optical spectroscopy of graphene: From the far infrared to the ultraviolet, *Solid State Commun.*, 2012, **152**(15), 1341–1349, DOI: **10.1016/j.ssc.2012.04.064**.

16 A. H. Castro Neto, F. Guinea, N. M. R. Peres, K. S. Novoselov and A. K. Geim, The electronic properties of graphene, *Rev. Mod. Phys.*, 2009, **81**(1), 109–162, DOI: **10.1103/RevModPhys.81.109**.

17 N. Engineering, R. M. Engineering and E. Toto, Functional nanocomposites based on graphene/DNA interface : Towards a bio-inspired sensing of UV radiation effects, no. 1187221.

18 A. C. M. De Moraes, *et al.*, Fabrication of transparent and ultraviolet shielding composite films based on graphene oxide and cellulose acetate, *Carbohydr. Polym.*, 2015, **123**, 217–227, DOI: **10.1016/j.carbpol.2015.01.034**.

19 X. Tang, *et al.*, Functionalization of cotton fabric with graphene oxide nanosheet and polyaniline for conductive and UV blocking properties, *Synth. Met.*, 2015, **202**, 82–88, DOI: **10.1016/j.synthmet.2015.01.017**.

20 M. Tian, X. Tang, L. Qu, S. Zhu, X. Guo and G. Han, Robust ultraviolet blocking cotton fabric modified with chitosan/graphene nanocomposites, *Mater. Lett.*, 2015, **145**, 340–343, DOI: **10.1016/j.matlet.2015.01.147**.

21 S. Pei and H. M. Cheng, The reduction of graphene oxide, *Carbon*, 2012, **50**(9), 3210–3228, DOI: **10.1016/j.carbon.2011.11.010**.

22 R. Trusovas, G. Račiukaitis, G. Niaura, J. Barkauskas, G. Valušis and R. Pauliukaite, Recent Advances in Laser Utilization in the Chemical Modification of Graphene Oxide and Its Applications, *Adv. Opt. Mater.*, 2016, **4**(1), 37–65, DOI: **10.1002/adom.201500469**.

23 Y. Zhu, *et al.*, Graphene and graphene oxide: Synthesis, properties, and applications, *Adv. Mater.*, 2010, **22**(35), 3906–3924, DOI: **10.1002/adma.201001068**.

24 K. P. Loh, Q. Bao, P. K. Ang and J. Yang, The chemistry of graphene, *J. Mater. Chem.*, 2010, **20**(12), 2277–2289, DOI: **10.1039/b920539j**.

25 X. Hu, X. Zhang, M. Tian, L. Qu, S. Zhu and G. Han, Robust ultraviolet shielding and enhanced mechanical properties of graphene oxide/sodium alginate composite films, *J. Compos. Mater.*, 2016, **50**(17), 2365–2374, DOI: **10.1177/0021998315603227**.

26 D. Yang, *et al.*, Chemical analysis of graphene oxide films after heat and chemical treatments by X-ray photoelectron and Micro-Raman spectroscopy, *Carbon*, 2009, **47**(1), 145–152, DOI: **10.1016/j.carbon.2008.09.045**.

27 R. Giardi, S. Porro, A. Chiolerio, E. Celasco and M. Sangermano, Inkjet printed acrylic formulations based on UV-reduced graphene oxide nanocomposites, *J. Mater. Sci.*, 2013, **48**(3), 1249–1255, DOI: **10.1007/s10853-012-6866-4**.

28 L. Guardia, S. Villar-Rodil, J. I. Paredes, R. Rozada, A. Martínez-Alonso and J. M. D. Tascón, UV light exposure of aqueous graphene oxide suspensions to promote their direct reduction, formation of graphene-metal nanoparticle hybrids and dye degradation, *Carbon*, 2012, **50**(3), 1014–1024, DOI: **10.1016/j.carbon.2011.10.005**.

29 M. Kotsidi, *et al.*, Preventing colour fading in artworks with graphene veils, *Nat. Nanotechnol.*, 2021, 1–7, DOI: **10.1038/s41565-021-00934-z**.

30 J. Zhu, X. Li, Y. Zhang, J. Wang and B. Wei, Graphene-Enhanced Nanomaterials for Wall Painting Protection, *Adv. Funct. Mater.*, 2018, **28**(44), 1–10, DOI: **10.1002/adfm.201803872**.

31 P. K. Panigrahi and A. Pathak, Microwave-assisted synthesis of WS2 nanowires through tetrathiotungstate precursors, *Sci. Technol. Adv. Mater.*, 2008, **9**(4), 045008–045013, DOI: **10.1088/1468-6996/9/4/045008**.

32 Y. Chen, L. Tan, M. Sun, C. Lu, J. Kou and Z. Xu, Enhancement of photocatalytic performance of TaON by combining it with noble-metal-free MoS2 cocatalysts, *J. Mater. Sci.*, 2019, **54**(7), 5321–5330, DOI: **10.1007/s10853-018-03214-9**.

33 G. Gao, *et al.*, Designing nanoscaled hybrids from atomic layered boron nitride with silver nanoparticle deposition, *J. Mater. Chem. A*, 2014, **2**(9), 3148–3154, DOI: **10.1039/c3ta12892j**.

This journal is © The Royal Society of Chemistry 2023

Open Access Article. Published on 23 February 2023. Downloaded on 8/16/2024 2:06:04 PM.
This article is licensed under a Creative Commons Attribution-NonCommercial 3.0 Unported Licence.

34 J. N. Coleman, *et al.*, Coleman2011.Pdf, *Science*, 2011, **331**, 568–571, [Online]. Available: **https://science.sciencemag.org/**.
35 J. Kim, *et al.*, Direct exfoliation and dispersion of two-dimensional materials in pure water via temperature control, *Nat. Commun.*, 2015, **6**, 1–9, DOI: **10.1038/ncomms9294**.
36 N. I. Kovtyukhova, P. J. Ollivier, B. R. Martin, T. E. Mallouk, E. V. Buzaneva and A. D. Gorchinskiy, Layer-by-layer assembly of ultrathin composite films from micron-sized graphite oxide sheets and polycations, *Chem. Mater.*, 1999, **11**(3), 771–778, DOI: **10.1021/cm981085u**.
37 W. S. Wyszecki and G. Stiles, *Color Science: Concepts and Methods, Quantitative Data and Formulae, 2nd ed*., Wiley Classics Library, New York, NY, 2000, vol. 2000.
38 Calculating the Energy from Sunlight over a 12-Hour Period. **https://www.grc.nasa.gov/www/k-12/Numbers/Math/Mathematical_Thinking/sun12.htm**.
39 National Optical Astronomy Observatory (NOAO), Recommended Light Levels, 2015, [Online]. Available: **https://www.noao.edu/education/QLTkit/ACTIVITY_Documents/Safety/LightLevels_outdoor+indoor.pdf**.
40 C. Pavlou, *et al.*, Effective EMI shielding behaviour of thin graphene/PMMA nanolaminates in the THz range, *Nat. Commun.*, 2021, **12**(1), 1–9, DOI: **10.1038/s41467-021-24970-4**.
41 G. Anagnostopoulos, *et al.*, Strain Engineering in Highly Wrinkled CVD Graphene/Epoxy Systems, *ACS Appl. Mater. Interfaces*, 2018, **10**(49), 43192–43202, DOI: **10.1021/acsami.8b14698**.
42 A. C. Ferrari and D. M. Basko, Raman spectroscopy as a versatile tool for studying the properties of graphene, *Nat. Nanotechnol.*, 2013, **8**(4), 235–246, DOI: **10.1038/nnano.2013.46**.
43 Y. Hernandez, *et al.*, High-yield production of graphene by liquid-phase exfoliation of graphite, *Nat. Nanotechnol.*, 2008, **3**(9), 563–568, DOI: **10.1038/nnano.2008.215**.
44 V. Paolucci, *et al.*, Sustainable Liquid-Phase Exfoliation of Layered Materials with Nontoxic Polarclean Solvent, *ACS Sustainable Chem. Eng.*, 2020, **8**(51), 18830–18840, DOI: **10.1021/acssuschemeng.0c04191**.
45 Substance Infocard 1-methyl-2-pyrrolidone. [Online]. Available: **https://echa.europa.eu/de/substance-information/-/substanceinfo/100.011.662**.
46 X. Cai, Z. Jiang, X. Zhang and X. Zhang, Effects of Tip Sonication Parameters on Liquid Phase Exfoliation of Graphite into Graphene Nanoplatelets, *Nanoscale Res. Lett.*, 2018, **13**, 241, DOI: **10.1186/s11671-018-2648-5**.
47 P. Brocos, J. Gracia-Fadrique, A. Amigo and Á. Piñeiro, Application of the Extended Langmuir model to surface tension data of binary liquid mixtures, *Fluid Phase Equilib.*, 2005, **237**(1–2), 140–151, DOI: **10.1016/j.fluid.2005.08.020**.
48 P. Oberschachtsiek, Surface tension values of some common test liquids for surface energy analysis Surface tension values of some common test liquids for surface energy analysis, *Dataphysics*, 2020, **49**(0), 0–4, [Online]. Available: **https://www.dataphysics-instruments.com**.
49 A. C. Ferrari, Raman spectroscopy of graphene and graphite: Disorder, electron-phonon coupling, doping and non-adiabatic effects, *Solid State Commun.*, 2007, **143**(1–2), 47–57, DOI: **10.1016/j.ssc.2007.03.052**.
50 S. Latil, V. Meunier and L. Henrard, Massless fermions in multilayer graphitic systems with misoriented layers: Ab initio calculations and experimental fingerprints, *Phys. Rev. B: Condens. Matter Mater. Phys.*, 2007, **76**(20), 1–4, DOI: **10.1103/PhysRevB.76.201402**.
51 J. Zeng, *et al.*, Irradiation effects of graphene and thin layer graphite induced by swift heavy ions, *Chin. Phys. B*, 2015, **24**(8), 086103–086109, DOI: **10.1088/1674-1056/24/8/086103**.
52 M. Wojtoniszak, *et al.*, Synthesis, dispersion, and cytocompatibility of graphene oxide and reduced graphene oxide, *Colloids Surf., B*, 2012, **89**(1), 79–85, DOI: **10.1016/j.colsurfb.2011.08.026**.
53 F. T. Johra, J. W. Lee and W. G. Jung, Facile and safe graphene preparation on solution based platform, *J. Ind. Eng. Chem.*, 2014, **20**(5), 2883–2887, DOI: **10.1016/j.jiec.2013.11.022**.
54 A. Ghorai, S. Bayan, N. Gogurla, A. Midya and S. K. Ray, Highly luminescent WS2 quantum dots/ZnO heterojunctions for light emitting devices, *ACS Appl. Mater. Interfaces*, 2017, **9**(1), 558–565, DOI: **10.1021/acsami.6b12859**.
55 B. Singh, *et al.*, Nanostructured Boron Nitride with High Water Dispersibility for Boron Neutron Capture Therapy, *Sci. Rep.*, 2016, **6**, 35535–35544, DOI: **10.1038/srep35535**.
56 R. Chua, *Optical transmission of 2D crystals and ultra thin black phosphorus*, National University of Singapore, 2016.
57 M. Xu, T. Liang, M. Shi and H. Chen, Graphene-like two-dimensional materials, *Chem. Rev.*, 2013, **113**(5), 3766–3798, DOI: **10.1021/cr300263a**.
58 T. History, Artists' Pigments: A Handbook of Their History and Characteristics, ed. Ashok Roy, vol. 2, 1993.
59 D. E. Mouzakis, H. Zoga and C. Galiotis, Accelerated environmental ageing study of polyester/glass fiber reinforced composites (GFRPCs), *Composites, Part B*, 2008, **39**(3), 467–475, DOI: **10.1016/j.compositesb.2006.10.004**.
60 N. Materials, Standard Practice for Operating Fluorescent Light Apparatus for UV Exposure of, *Technology*, 2001, 1–9.
61 S. Rao, J. Upadhyay, K. Polychronopoulou, R. Umer and R. Das, Reduced graphene oxide: Effect of reduction on electrical conductivity, *J. Compos. Sci.*, 2018, **2**(2), 25–36, DOI: **10.3390/jcs2020025**.
62 J. E. Mates, *et al.*, Durable and flexible graphene composites based on artists' paint for conductive paper applications, *Carbon*, 2015, **87**(C), 163–174, DOI: **10.1016/j.carbon.2015.01.056**.
63 T. C. Dos Santos, G. J. Zocolo, D. A. Morales, G. de A. Umbuzeiro and M. V. B. Zanoni, Assessment of the breakdown products of solar/UV induced photolytic degradation of food dye tartrazine, *Food Chem. Toxicol.*, 2014, **68**, 307–315, DOI: **10.1016/j.fct.2014.03.025**.
64 Y. Qiu, *et al.*, Antioxidant chemistry of graphene-based materials and its role in oxidation protection technology, *Nanoscale*, 2014, **6**(20), 11744–11755, DOI: **10.1039/c4nr03275f**.

Open Access Article. Published on 23 February 2023. Downloaded on 8/16/2024 2:06:04 PM.
This article is licensed under a Creative Commons Attribution-NonCommercial 3.0 Unported Licence.

65 N. Nuraje, S. I. Khan, H. Misak and R. Asmatulu, The Addition of Graphene to Polymer Coatings for Improved Weathering, *ISRN Polym. Sci.*, 2013, **2013**, 1–8, DOI: 10.1155/2013/514617.

66 Y. Su, V. G. Kravets, S. L. Wong, J. Waters, A. K. Geim and R. R. Nair, Impermeable barrier films and protective coatings based on reduced graphene oxide, *Nat. Commun.*, 2014, **5**, 1–5, DOI: 10.1038/ncomms5843.

67 S. A. Everett, M. F. Dennis, K. B. Patel, S. Maddix, S. C. Kundu and R. L. Willson, Scavenging of nitrogen dioxide, thiyl, and sulfonyl free radicals by the nutritional antioxidant β-carotene, *J. Biol. Chem.*, 1996, **271**(8), 3988–3994, DOI: 10.1074/jbc.271.8.3988.

68 Y. Qin and R. A. Wheeler, Density-functional-derived structures, spin properties, and vibrations for phenol radical cation, *J. Phys. Chem.*, 1996, **100**(25), 10554–10563, DOI: 10.1021/jp952886c.

69 B. R. Bitner, *et al.*, Antioxidant carbon particles improve cerebrovascular dysfunction following traumatic brain injury, *ACS Nano*, 2012, **6**(9), 8007–8014, DOI: 10.1021/nn302615f.

70 F. Kar, *et al.*, Hexagonal boron nitride nanoparticles trigger oxidative stress by modulating thiol/disulfide homeostasis, *Hum. Exp. Toxicol.*, 2021, **40**(9), 1572–1583, DOI: 10.1177/09603271211002892.

71 E. Czarniewska, L. Mrówczyńska, M. Jędrzejczak-Silicka, P. Nowicki, M. Trukawka and E. Mijowska, Non-cytotoxic hydroxyl-functionalized exfoliated boron nitride nanoflakes impair the immunological function of insect haemocytes in vivo, *Sci. Rep.*, 2019, **9**(1), 1–15, DOI: 10.1038/s41598-019-50097-0.

72 L. H. Li and Y. Chen, Atomically Thin Boron Nitride: Unique Properties and Applications, *Adv. Funct. Mater.*, 2016, **26**(16), 2594–2608, DOI: 10.1002/adfm.201504606.

73 A. Falin, *et al.*, Mechanical properties of atomically thin boron nitride and the role of interlayer interactions, *Nat. Commun.*, 2017, **8**, 1–9, DOI: 10.1038/ncomms15815.

74 S. Thakur, P. Bandyopadhyay, S. H. Kim, N. H. Kim and J. H. Lee, Enhanced physical properties of two dimensional MoS2/poly(vinyl alcohol) nanocomposites, *Composites, Part A*, 2018, **110**, 284–293, DOI: 10.1016/j.compositesa.2018.05.009.

75 C. Y. Tsai, S. Y. Lin and H. C. Tsai, Butyl rubber nanocomposites with monolayer MoS2 additives: Structural characteristics, enhanced mechanical, and gas barrier properties, *Polymers*, 2018, **10**(3), 238–250, DOI: 10.3390/polym10030238.

76 A. Falin, *et al.*, Mechanical Properties of Atomically Thin Tungsten Dichalcogenides: WS2, WSe2, and WTe2, *ACS Nano*, 2021, **15**(2), 2600–2610, DOI: 10.1021/acsnano.0c07430.

77 J. H. Park, *et al.*, Selective Chemical Response of Transition Metal Dichalcogenides and Metal Dichalcogenides in Ambient Conditions, *ACS Appl. Mater. Interfaces*, 2017, **9**(34), 29255–29264, DOI: 10.1021/acsami.7b08244.

78 C. Zhang, *et al.* No Electrical transport properties of individual WS 2 nanotubes and their dependence on water and oxygen absorptionTitle, *Appl. Phys. Lett.*, 2012, **101**, 8174–8181, DOI: 10.1063/1.4752440.

79 R. Y. N. Gengler, *et al.*, Revealing the ultrafast process behind the photoreduction of graphene oxide, *Nat. Commun.*, 2013, **4**, 1–5, DOI: 10.1038/ncomms3560.

80 J. Yan, Y. Zhang, P. Kim and A. Pinczuk, Electric field effect tuning of electron-phonon coupling in graphene, *Phys. Rev. Lett.*, 2007, **98**(16), 1–4, DOI: 10.1103/PhysRevLett.98.166802.

81 C. Mattevi, *et al.*, Evolution of electrical, chemical, and structural properties of transparent and conducting chemically derived graphene thin films, *Adv. Funct. Mater.*, 2009, **19**(16), 2577–2583, DOI: 10.1002/adfm.200900166.

82 T. Dutta, *et al.*, ROS generation by reduced graphene oxide (rGO) induced by visible light showing antibacterial activity: Comparison with graphene oxide (GO), *RSC Adv.*, 2015, **5**(98), 80192–80195, DOI: 10.1039/c5ra14061g.

83 X. Gao, J. Jang and S. Nagase, Hydrazine and thermal reduction of graphene oxide: Reaction mechanisms, product structures, and reaction design, *J. Phys. Chem. C*, 2010, **114**(2), 832–842, DOI: 10.1021/jp909284g.

This journal is © The Royal Society of Chemistry 2023